INFLUENCE OF INTERCELLULAR CLEFTS ON POTENTIAL AND CURRENT DISTRIBUTION IN A MULTIFIBER PREPARATION

H. G. HAAS AND G. BROMMUNDT, *Second Institute of Physiology, University of Bonn, D 53 Bonn, Federal Republic of Germany*

ABSTRACT A theoretical model is presented for current and voltage clamp of multifiber bundles in a double sucrose gap. Attention is focused on methodological errors introduced by the intercellular cleft resistance. The bundle is approximated by a continuous geometry. Voltage distribution, as a function of radial distance and time, is defined by a parabolic partial differential equation which is specified for different membrane characteristics. Assuming a linear membrane, analytical solutions are given for current step and voltage step conditions. The theoretical relations (based on Bessel functions) may be used to calculate membrane conductance and capacity from experimental clamp data. The case of a nonlinear membrane with standard Hodgkin-Huxley kinetics for excitatory Na current is treated assuming maximum Na conductances ($\bar{g}_{Na}$) of 120, 10, and 1 mmho/cm^2. Numerical simulations are presented for potential and current distribution in a bundle of 60 μm diameter during depolarizing voltage steps. Adequate voltage control is restricted to the peripheral fibers of the bundle whereas the membrane potential of the inner fibers deviates from the command level during early inward current, tending to the Na equilibrium potential. In the peak current-voltage diagram the loss of voltage control is reflected by an increased steepness of the negative region and a decreased slope conductance of the positive region. With $\bar{g}_{Na} = 120$ mmho/cm^2, the positive slope conductance is ~25% of the slope expected from ideal space clamping. With the lower values of $\bar{g}_{Na}$, the slope conductance ratio is in the order of 50%. Implications of the results for an experimental voltage clamp analysis of early inward current on multifiber preparations are discussed.

INTRODUCTION

Recent attempts to use the sucrose gap technique for voltage clamping of cardiac or smooth muscle bundles have been severely criticized by several authors (Johnson and Lieberman, 1971; Kootsey and Johnson, 1972; Tarr and Trank, 1974, 1976; McGuigan, 1974; Ramón et al., 1975). The multicellular nature of a bundle implies a number of complications as compared with a single fiber preparation. A main problem is the presence of an appreciable extracellular resistance which resides in the intercellular clefts. When a command signal is applied between the bundle surface and the interior of the cells, the current flow related to the deeper-lying fibers will produce a voltage drop across the cleft resistance and may cause large deviations of the transmembrane potential from the command voltage. A quantitative analysis of the errors induced by the cleft resistance is difficult because of the distributed arrangement of the extracellular pathways. As a rough approximation, the bundle may be represented by a single unidimensional cable with a lumped series resistance (Kootsey and Johnson, 1972; Ramón et al., 1975). A lumped approximation of cleft resistance was also used by Jakobsson

et al. (1975) who considered a bundle as made up of three coaxial layers of fibers associated with different extracellular resistances to radial current flow. A more general treatment was given by Attwell and Cohen (1977) on the basis of a statistical approach. In their model the preparation was represented by a large number of unidimensional cables in parallel, and the radial voltage distribution across the bundle during a step clamp was calculated by an averaging procedure, i.e. the discrete arrangement of fibers and clefts was approximated by a continuum.

The present paper follows a concept similar to that used by Attwell and Cohen (1977). The aim of the study is to describe the transmembrane voltage in a bundle as a function of radial distance and time under voltage or current clamp conditions, and to evaluate the influence of external parameters (bundle diameter, cleft width, external resistivity) on potential and current distribution. This is done for the case of a linear membrane and for an active, nonlinear membrane endowed with a Na kinetics of the Hodgkin-Huxley (1952 *b*) type. The case of a linear membrane results in a partial differential equation which is solved by analytical procedures. The case of an active membrane is described by a set of differential equations which require numerical computation.

THE THEORETICAL MODEL

The typical features of a multicellular preparation in a double sucrose gap voltage clamp arrangement are illustrated in Fig. 1A. A short segment in the middle of the bundle is flanked by two sucrose streams generating an extracellular insulation. This segment is perfused with the test solution. The two ends of the preparation are immersed in isotonic KCl solution. Membrane voltage in the test node is controlled by a feedback circuitry. Gross electrodes are used for voltage recording and current injection. The membrane potential in the test segment is measured as the transgap potential at one end of the bundle. Controlling current is injected into all fibers at the other end of the bundle, leaves the fibers by crossing the membranes in the test node, and is collected by a central electrode. The current leaving the interior fibers passes through a number of intercellular clefts before it reaches the bundle surface.

For our model the following simplifying assumptions are made. The test node is regarded as a short segment of a cylindrical bundle (radius a) with well-defined boundaries at the two ends. Intermixing between sucrose and test solution in the interior of the preparation is neglected. The sucrose insulation is assumed perfect. The test node is represented by a large number of parallel fibers of identical shape and membrane properties. It is assumed that the individual fibers have full bundle length and intercellular connections do not exist. The fibers are considered to have a hexagonal cross-section; the length of side (b) is half the diameter of the fibers. The distance between adjacent fibers (d) is constant throughout the preparation. The intercellular space is filled with a fluid of conductivity σ_e. In a cross-section of the bundle the intercellular clefts form a regular network. The external medium is taken as a volume conductor of zero resistance which is in immediate contact with the outermost layer of fibers. We assume that the intracellular potential is constant in all fibers and take this to be zero. Thus the cleft potential is equal and opposite to the membrane potential in its conventional definition. Membrane current is taken positive if directed inward. Any axial nonuniformity of potential is ignored, i.e., extracellular current flow is only in a plane normal to the bundle axis. Technical limitations of the voltage clamp circuit are neglected; the time required for a step

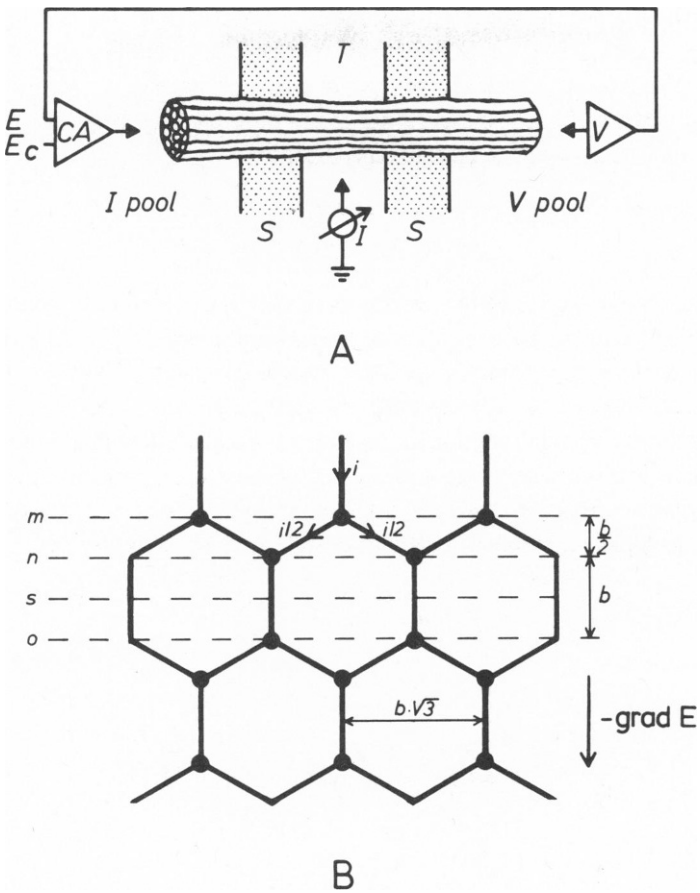

FIGURE 1 (A) Multifiber preparation in a double sucrose gap voltage clamp apparatus as designed by Julian et al. (1962*a*,*b*); schematic diagram. S: sucrose partitions; T: test compartment; CA: control amplifier; V: voltage recording device; E_c: command signal; I: operational amplifier in currentometric mode. For current clamp experiments, the control amplifier is replaced by a constant current source. (B) Symmetrical current flow through the cleft network. Current strength is i in the main flow direction (from top to bottom) and $i/2$ in the other branches of the network. Homologous nodal points are at the same potential. The voltage gradient between the planes m and n is the same as that between n and o. Equivalent current density, j, equals $i/(lb\sqrt{3})$ where l is the length of the test node.

change in voltage is regarded as infinitesimal. When a command voltage is applied between the bathing medium and the interior of the cells, adequate voltage control is expected for the superficial fibers of the bundle. The membrane potential of an interior fiber, however, will deviate from the command voltage by an amount equal to the voltage drop along any extracellular pathway connecting the fiber to the bundle surface.

For a calculation of voltage and current distribution in the bundle the truly distributed structures are transformed into an appropriate continuous system. The procedure is similar to that employed by Adrian et al. (1969) in their analysis of potential and current spread in the transverse tubular system of skeletal muscle (cf. Fig. 11 in their paper). First, the network of the intercellular clefts is converted to an equivalent cylinder and the actual conductivity of the

extracellular fluid is substituted by an effective conductivity of the bundle as a whole. The principle is illustrated in Fig. 1B. We consider the simplified situation that cleft current flow is symmetrical to one main axis of the hexagonal network, neglecting current sources or sinks. By a uniform spread of the cleft currents over plane (s) we obtain an equivalent current density, j, which is related to the cleft potential, E, by

$$j = -\frac{d\sigma_e}{b\sqrt{3}} \operatorname{grad} E. \tag{1}$$

The term $d\sigma_e/(b\sqrt{3})$ signifies the effective conductivity for continuous current flow, $\bar{\sigma}$. Because any cleft current pattern may be approximated by the sum of three symmetrical currents related to the three main axis of the hexagonal system, we take Eq. 1 as the general relation between extracellular current and affiliated field.

To complete the model, membrane currents as the sources of cleft current are incorporated. A change of the extracellular current along a cleft equals the amount of current entering or leaving the adjacent fibers. For $d \ll b$, the membrane area per unit volume of the bundle is $4/(b\sqrt{3})$. Denoting the membrane current per unit area of cell membrane by

$$i_m = i_{\text{ion}} + C_m \frac{\partial E}{\partial t}$$

we obtain

$$\operatorname{div} j = -\frac{4}{b\sqrt{3}}\left(i_{\text{ion}} + C_m \frac{\partial E}{\partial t}\right). \tag{2}$$

Combining Eqs. 1 and 2 yields

$$\Delta E = \frac{4}{d\sigma_e}\left(i_{\text{ion}} + C_m \frac{\partial E}{\partial t}\right), \tag{3}$$

where Δ is the Laplace operator. Eq. 3 may be considered a simplified version of more general differential equations describing the spread of potential in three-dimensional syncytia in which the intracellular space is not isopotential (Eisenberg et al., 1979; Peskoff, 1979*a*,*b*). Assuming a cylindrical symmetry of voltage distribution Eq. 3 may be written

$$\frac{\partial^2 E}{\partial r^2} + \frac{1}{r}\frac{\partial E}{\partial r} = \frac{4}{d\sigma_e}\left(i_{\text{ion}} + C_m \frac{\partial E}{\partial t}\right), \tag{4}$$

where r is the radial distance from the bundle axis. This is the general equation governing the potential spread in our continuous model. (Note that this relation is independent of the fiber radius b.) Formally it is the cylindrical analogue of the one-dimensional cable equation, the difference being the occurrence of the term $1/r\ \partial E/\partial r$ on the left-hand side. To give Eq. 4 a definite meaning the term i_{ion} must be specified according to the membrane properties. The simplest case is i_{ion} being a linear function of membrane potential as is expected for small de- or hyperpolarizations from the resting potential. The ionic current flow through a passive membrane equals $G_m u$ where G_m is the resting membrane conductance and u the displace-

ment of the membrane potential from its resting value. Eq. 4 then becomes

$$\frac{\partial^2 u}{\partial r^2} + \frac{1}{r}\frac{\partial u}{\partial r} = k^2\left(u + \tau\frac{\partial u}{\partial t}\right), \tag{5}$$

where $k^2 = 4G_m/(d\sigma_e)$ and $\tau = C_m/G_m$. The constant k is analogous to the reciprocal of a space constant as used in linear cable theory and τ is the membrane time constant. Eq. 5 is equivalent to the Adrian et al. (1969) Eq. 9.

RESULTS

Linear Membrane; Steady-State Solution

For a time-independent situation, Eq. 5 reduces to

$$\frac{d^2 u}{dr^2} + \frac{1}{r}\frac{du}{dr} = k^2 u. \tag{5a}$$

Setting $R = rk$ we obtain the dimensionless equation

$$\frac{d^2 u}{dR^2} + \frac{1}{R}\frac{du}{dR} = u. \tag{5b}$$

This is a modified Bessel equation of zero order, and its solutions are given by appropriate combinations of the Bessel functions $I_o(R)$ and $K_o(R)$. Because $u(R)$ remains finite at $R = 0$, the solution of Eq. 5*b* is a multiple of $I_o(R)$. If u_a is the potential at the surface of the bundle ($r = a$), the voltage distribution inside the bundle is given by

$$u(r) = u_a\frac{I_o(rk)}{I_o(ak)} = u_a\frac{I_0\left(\frac{r}{a}ak\right)}{I_o(ak)}. \tag{6}$$

The solution is characterized by the dimensionless parameter $(ak) = (2a/\sqrt{d}) \times \sqrt{G_m/\sigma_e}$, which may be interpreted as the product of two terms representing the morphological and electrical properties of the preparation, respectively. The larger the numerical value of (ak), the greater is the voltage inhomogeneity in the interior of the bundle. Assuming fixed values of G_m and σ_e, the potential distribution, as a function of r/a, is fully determined by the ratio of bundle radius (a) to square root of cleft width ($\sqrt{d}$).

To illustrate the features of the radial voltage profile, we shall apply Eq. 6 to frog atrial muscle, a preparation which is widely used in cardiac voltage clamping. In this tissue the individual fibers are long tapering cells which are grouped in bundles (or trabeculae) of a diameter between 30 and 100 μm (Barr et al., 1965; Baldwin, 1970; Connor et al., 1975). (According to Page and Niedergerke [1972] frog heart trabeculae are surrounded by an endothelial layer which represents a resistance to radial current flow in the order of 40 Ωcm^2. Because this component of extracellular resistance may be minimized by electronic compensation, it is neglected in this study.) The following values are adopted for the morphological and electrical parameters of frog atrial muscle: a, bundle radius, 3×10^{-3} cm (= 30 μm); d, cleft width, 3×10^{-6} cm (= 0.03 μm); σ_e, conductivity of the external medium (taken as Ringer's fluid), 12 mmho/cm.

Steady membrane conductance, G_m, is thought to range between 0.1 and 50 mmho/cm^2. In Fig. 2A, the steady membrane potential as calculated from Eq. 6 is plotted vs. the radial distance for nine different values of G_m. Resting membrane conductance under normal conditions is assumed to lie between 0.1 and 1 mmho/cm^2 (Connor et al., 1975; Attwell and Cohen, 1977). For those low values of G_m the voltage distribution across the bundle does not greatly deviate from homogeneity. With increasing values of G_m—as are expected e.g. with elevated levels of external potassium—a striking loss of voltage control occurs in the interior fibers of the bundle.

It should be stressed that intercellular clefts as narrow as 0.03 μm are not typical of all cardiac structures. Much wider clefts have been observed in mammalian heart muscle. For example, in rabbit Purkinje strands the individual fibers are spaced ~1 μm apart (Sommer and Johnson, 1968) and clefts up to 3 μm may exist in ventricular preparations of larger mammals. Obviously in such a preparation the cleft resistance (per unit length) is distinctly lower and the voltage drop related to extracellular current flow will be much smaller than in a frog atrial bundle. In a tissue with very wide clefts, larger bundle diameters may be tolerated at a given voltage error. This is easy to verify from Eq. 6. Because the potential distribution in a fiber bundle is determined by the $a/\sqrt{d}$ ratio, the same voltage deviation (u/u_a) as in a frog atrial bundle is expected for a mammalian ventricular preparation with a cleft width 100 times and a bundle radius 10 times as large (provided that the electrical parameters G_m and σ_e are the same in both tissues).

Eq. 6 does not only hold for resting membrane conditions but is applicable to any steady or quasi-steady state of the membrane. The general effect of a cleft resistance in a voltage-clamped fiber bundle is to shift the membrane potential of the inner fibers from the command level towards the intrinsic electromotive force of the membrane, i.e., the reversal potential of total membrane current or equilibrium potential (Shanes, 1958; FitzHugh, 1960). During

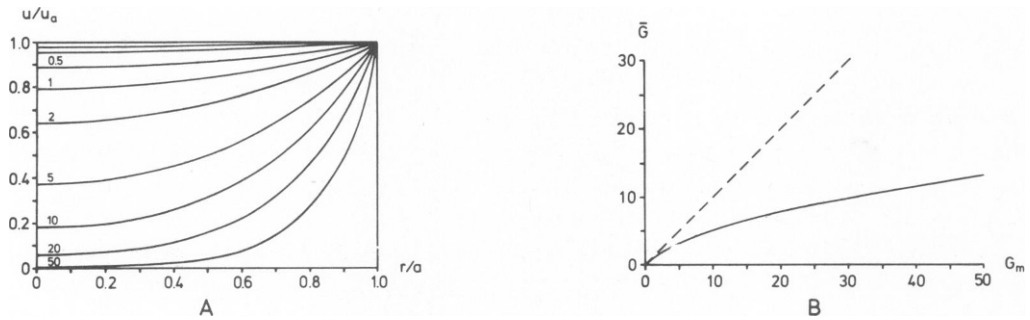

FIGURE 2 (A) Steady potential distribution in a frog atrial bundle during long-lasting voltage or current clamp at different values of membrane conductance. The abscissa is the radial distance (r) from bundle axis relative to the bundle radius (a). The ordinate is the potential displacement u at r expressed as fraction of the potential displacement u_a at the bundle surface. The numbers against the curves are the membrane conductances (G_m) in millimhos per square centimeter. The two top curves refer to conductances of 0.1 and 0.2 mmho/cm^2, respectively. (B) Full line: Apparent membrane conductance ($\bar{G}$) of a frog atrial preparation as function of actual membrane conductance (G_m), calculated from Eq. 8b. Conductances are given in millimhos per square centimeter. Broken line: Ideal relation ($\bar{G} = G_m$) as expected in the absence of any cleft resistance.

excitation, the electromotive force of the membrane is mainly represented by an Na battery. When a superthreshold depolarizing clamp is applied to a fiber bundle, the membrane potential of the inner fibers will swing toward the Na equilibrium potential, E_{Na}, thus producing some kind of potential spike. As a rough approximation, one may assume that all fibers of the bundle would reach the same value of peak Na conductance, g_p, at the same time. The peak voltage distribution in the bundle may then be considered to be near a steady state and Eq. 6 may be used to estimate the amount of voltage deviation of the inner fibers, setting $u = (E - E_{Na})$, $u_a = (E_{clamp} - E_{Na})$ and $G_m = g_p$. An example of a peak voltage profile analyzed in this way is given in Fig. 6.

Considering the bundle as a whole, the central fibers (with the highest voltage deviation) represent only a relatively small fraction of the total fiber population. The mean value of the membrane potential of all fibers in the bundle is given by

$$\bar{u} = u_a \int_{r=0}^{a} \frac{I_o(rk)}{I_o(ak)} \frac{2\pi r}{\pi a^2} dr. \tag{7a}$$

Now $\int_{z=0}^{\zeta} zI_o(z)\,dz = \zeta I_1(\zeta)$ where $I_1(z)$ is the hyperbolic Bessel function of first order. Thus Eq. 7*a* can be written

$$\bar{u} = u_a \frac{2}{ak} \frac{I_1(ak)}{I_o(ak)}. \tag{7b}$$

Accordingly, the mean value of membrane current density (referred to actual membrane area) is

$$I_m = G_m \bar{u} = G_m u_a \frac{2}{ak} \frac{I_1(ak)}{I_o(ak)}. \tag{8a}$$

This is equivalent to the current-voltage relation in the tubular model of Adrian et al. (1969; Eq. 12). The term $2I_1(ak)/akI_o(ak)$ is between zero (for large values of G_m) and one (for very small G_m). It represents the alteration of the current-voltage relation caused by the cleft resistance. From Eq. 8*a* we obtain the apparent membrane conductance

$$\bar{G} = \frac{I_m}{u_a} = G_m \frac{2}{ak} \frac{I_1(ak)}{I_o(ak)}. \tag{8b}$$

The definition of conductance by the I_m:u_a ratio is analogous to the practical value of conductance as it results from a straight-forward evaluation of experimental clamp data. Fig. 2 B illustrates the dependence of $\bar{G}$ (or of I_m at a given voltage u_a) on G_m. For sufficiently low values of membrane conductance, the radial voltage gradient across the bundle is negligibly small; I_m is almost linearly related to G_m, and $\bar{G}$ is close to G_m. With increasing membrane conductance, the voltage gradient increases; the relation between I_m and G_m deviates from linearity so that $\bar{G} < G_m$. This error, however, is distinctly smaller than one would expect from an unreflected inspection of the voltage profiles shown in Fig. 2A. With a membrane conductance of 10 mmho/cm^2, the deviation of $\bar{G}$ from G_m is ~50% although the voltage control in the interior of the bundle is rather poor. For very high values of G_m, the term $I_1(ak)/I_o(ak)$ approaches unity and

$$\bar{G} \to G_m \frac{2}{2a\sqrt{G_m/(d\sigma_e)}} = \frac{1}{a}\sqrt{G_m d\sigma_e}, \tag{8c}$$

i.e., $\bar{G}$ becomes related to the square root of G_m (cf. Attwell and Cohen, 1977, Eq. 34).

Linear Membrane; Transient Response to Current Step

Time-dependent solutions of Eq. 5 are derived by use of the Laplace transformation. Denoting the Laplace transform of $u(r, t)$ by $U(r, s)$ we obtain from Eq. 5 the ordinary differential equation

$$\frac{d^2U}{dr^2} + \frac{1}{r}\frac{dU}{dr} = k^2[U + \tau sU - \tau u_o(r)], \tag{9}$$

where s is the Laplace variable and $u_o(r)$ is the voltage distribution at $t = 0$ (initial condition of eq. 5). Assuming $u_o(r) = 0$ for all r the transformed equation reduces to

$$\frac{d^2U}{dr^2} + \frac{1}{r}\frac{dU}{dr} = \kappa^2 U, \tag{10}$$

where $\kappa^2 = k^2(1 + \tau s)$. Eq. 10 is formally equivalent to Eq. 5*a* and its solution is

$$U(r, s) = CI_o(r\kappa), \tag{11}$$

where C is a function of s. The dependence of C on s is determined by the boundary conditions of the current or voltage application. If a current of unity strength is applied to the bundle at time $t = 0$, the boundary condition is

$$2\pi al\bar{\sigma}\frac{\partial u}{\partial r}(a, t) = 1 \quad \text{or} \quad \frac{\partial u}{\partial r}(a, t) = A \quad \text{for all } t > 0, \tag{12}$$

where l is the length of the test node and $A = 1/(2\pi al\bar{\sigma})$. (Like membrane current, clamp current is taken positive if directed inward.) The Laplace transform of Eq. 12 is

$$\frac{dU}{dr}(a, s) = \frac{A}{s}. \tag{12a}$$

From Eq. 11

$$\frac{dU}{dr}(a, s) = C\kappa I_1(a\kappa),$$

so that

$$C = \frac{A}{s\kappa I_1(a\kappa)}.$$

Thus we have

$$U(r, s) = \frac{A}{s\kappa}\frac{I_o(r\kappa)}{I_1(a\kappa)} = \frac{A}{sk\sqrt{1 + \tau s}}\frac{I_o(rk\sqrt{1 + \tau s})}{I_1(ak\sqrt{1 + \tau s})}. \tag{13}$$

To obtain the original function $u(r, t)$ from the transform $U(r, s)$ we make use of the Bromwich integral

$$u(r, t) = \frac{1}{2\pi j} \oint U(r, s)\, e^{ts}\, ds,$$

where the integration is taken over an appropriate contour including all the poles s_ν of the integrand in the complex s-plane. The poles correspond to the zeros of the denominator in Eq. 13. As the result of the integration, $u(r, t)$ is expressed in the form

$$u(r, t) = \sum_{\nu=0}^{\infty} R_\nu(r, t), \tag{14}$$

where R_ν is the residue of $U(r, s)\, e^{ts}$ at the pole s_ν. The respective poles and residues are the following:

(a) The point $s_o = 0$ with

$$R_o = \frac{A}{k} \frac{I_o(rk)}{I_1(ak)}; \tag{14a}$$

(b) the zeros s_ν of $I_1(ak\sqrt{1 + \tau s})$ with the residues

$$R_\nu = \frac{2\, Ae^{s_\nu t}}{ak^2 \tau s_\nu} \frac{J_o\left(\frac{r}{a}\alpha_\nu\right)}{J_o(\alpha_\nu)} \quad (\nu = 1, 2 \ldots) \tag{14b}$$

where $J_o(z)$ is the unmodified Bessel function of zero order and the α_ν are the positive zeros of the Bessel function of first order, $J_1(z)$, beginning with $\alpha_1 = 0$. This means that α_2 corresponds to $j_{1,1} = 3.83$ in conventional terminology; in general, $\alpha_\nu = j_{1,\nu-1}$ for $\nu > 1$. The correlation between s_ν and α_ν is given by

$$s_\nu = -\frac{1}{\tau}\left[\left(\frac{\alpha_\nu}{ak}\right)^2 + 1\right].$$

(For details of the calculus of residues, see Doetsch, 1967, p. 138.)

The term R_o represents the steady-state distribution of membrane potential, $u_\infty(r)$, and becomes identical to the formulation given in Eq. 6 when the constant A is expressed by Eq. 8a. (A clamp current of unity strength is equivalent to a mean membrane current density of $b\sqrt{3}/4\pi a^2 l$.) The other terms R_ν are exponentials decreasing with time, the respective time constants being

$$\tau_\nu = -\frac{1}{s_\nu} = \tau \Big/ \left[\left(\frac{\alpha_\nu}{ak}\right)^2 + 1\right].$$

Using an abbreviated notation the potential distribution may be written

$$u(r, t) = u_\infty(r) \sum_{\nu=1}^{\infty} A_\nu(r)[1 - e^{-t/\tau_\nu}] \tag{15}$$

where

$$A_\nu = \frac{2ak}{\alpha_\nu^2 + (ak)^2} \frac{J_o\left(\frac{r}{a}\alpha_\nu\right)}{J_o(\alpha_\nu)} \frac{I_1(ak)}{I_o(rk)} \quad \text{and} \quad \sum_{\nu=1}^{\infty} A_\nu = 1.$$

The sign of A_ν may be positive or negative, depending on the particular values of α_ν and r/a.

Fig. 3 A illustrates the voltage response to a step current input as it develops with time in a frog atrial preparation. The top curve is identical to the steady-state voltage profile shown in Fig. 2 A (G_m = 1 mmho/cm^2). The potential in the center of the bundle reaches half its final value in ~0.8 ms. At the surface of the preparation half-time is ~0.6 ms. Obviously the higher the membrane conductance, the faster the charging process will be. Fig. 3 B shows the time-courses of membrane potential change at the bundle surface for different values of G_m. In all cases the final part of the charging is governed by the respective membrane time constant, $\tau = \tau_1 = C_m/G_m$. This corresponds to the linear part of the semilog plot in Fig. 3 B. The other exponentials involved ($\nu > 1$), with time constants $\tau_\nu < \tau$, are represented by the initial, upward concave part of the plot. For very low membrane conductances, the step

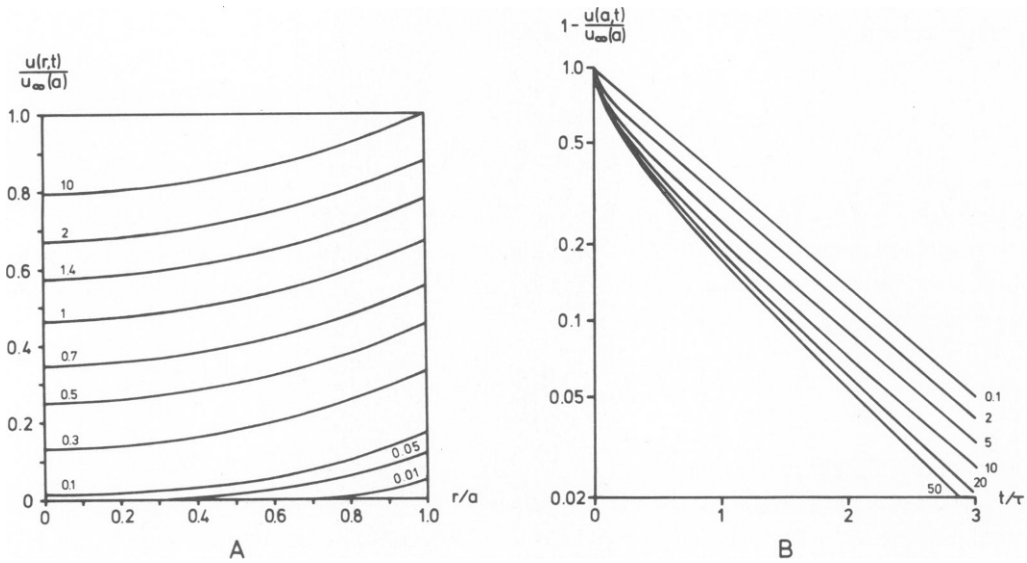

FIGURE 3 (A) Potential distribution across a frog atrial bundle at various times after application of a constant current pulse, calculated from Eq. 15. Abscissa: radial distance as fraction of bundle radius; ordinate: potential displacement relative to the steady potential displacement at the bundle surface ($r = a$). Curves are labeled by the times (in milliseconds) after onset of step current. Membrane conductance (G_m): 1 mmho/cm^2; membrane capacitance (C_m): 1 μF/cm^2. For times longer than 0.3 ms the curves are almost parallel. This is because voltage at those times is only determined by the terms R_o and R_1 in Eq. 14 and R_1 is independent of r. (B) Effect of membrane conductance (G_m) on transient voltage response generated by step current input to a frog atrial preparation. Abscissa: time after onset of current in units of the respective membrane time constants ($\tau = C_m/G_m$); ordinate: potential change of the superficial fibers, expressed as difference between instantaneous and steady potential divided by the steady potential (log scale). Lines are drawn according to Eq. 15 for $r = a$ and different values of G_m as indicated at the end of each curve (in millimhos per square centimeters). - In the numerical calculations used for this and the following figure, summation of the first 20 terms of the solution series ensured an accuracy of 99%.

current response approaches a simple exponential. With increasing values of G_m, the relative contribution of the faster exponentials becomes more pronounced. At $t = \tau$, charging is 63% complete at very low conductances but may reach >80% of the steady level at high conductances.

Linear Membrane; Transient Response to Voltage Step

When a constant voltage u_a is applied to the bundle surface at time $t = 0$, starting from initial zero conditions, the boundary condition of the transformed Eq. 10 becomes

$$U(a, s) = \frac{u_a}{s}. \tag{12b}$$

Using an analytical procedure analogous to that described in the previous section, we obtain the solution of the original Eq. 5 again in the form of an infinite series

$$u(r, t) = \sum_{\nu=0}^{\infty} R_\nu(r, t), \tag{16}$$

where

$$R_o = u_a \frac{I_o(rk)}{I_o(ak)} \tag{16a}$$

is the steady-state voltage distribution, $u_\infty(r)$, and the other terms are transients defined by

$$R_\nu = \frac{2u_a\beta_\nu e^{s\nu t}}{(ak)^2\tau s_\nu} \frac{J_o\left(\frac{r}{a}\beta_\nu\right)}{J_1(\beta_\nu)} \quad (\nu = 1, 2 \ldots). \tag{16b}$$

In this notation the β_ν are the positive roots of $J_o(z) = 0$ (starting with $\beta_1 \sim 2.4$) and

$$s_\nu = -\frac{1}{\tau}\left[\left(\frac{\beta_\nu}{ak}\right)^2 + 1\right].$$

The series may be rearranged to

$$u(r, t) = u_\infty(r) \sum_{\nu=1}^{\infty} B_\nu(r)[1 - e^{-t/\tau_\nu}], \tag{17}$$

where

$$B_\nu = \frac{-2\beta_\nu}{(ak)^2\tau s_\nu} \frac{J_o\left(\frac{r}{a}\beta_\nu\right)}{J_1(\beta_\nu)} \frac{I_o(ak)}{I_o(rk)}; \quad \sum_{\nu=1}^{\infty} B_\nu = 1 \text{ for } r < a$$

and

$$\tau_\nu = -\frac{1}{s_\nu} = \tau \Big/ \left[\left(\frac{\beta_\nu}{ak}\right)^2 + 1\right].$$

Current density at the bundle surface is

$$j_{\text{clamp}} = \bar{\sigma} u_a \left[\frac{k I_1(ak)}{I_o(ak)} - \sum_{\nu=1}^{\infty} \frac{2\beta_\nu^2 e^{s_\nu t}}{a^3 k^2 \tau s_\nu} \right]. \tag{18}$$

Eqs. 16*a,b* and 18 are equivalent to Eqs. 17 and 18 in the paper of Adrian et al. (1969).

Fig. 4 *A* shows computed solutions to Eq. 17 for various times after application of a step voltage to a frog atrial bundle. About 0.18 ms are required to bring the potential at the center to half its steady-state value and the potential change is >95% complete after 0.5 ms. With increasing radial distance from the bundle axis, the speed of the charging process increases; for $r = 15$ μm the half-time comes to ~0.13 ms. A comparison of Figs. 4 A and 3 A shows that the response to a step voltage approaches the steady level much faster than does the response to a step current. This is a result of the fact that there is no delay in charging the capacitance at $r = a$ and a very short delay for the fibers near the surface. The rate of charging is not very dependent on membrane conductance. Fig. 4 B illustrates the time-courses of potential at the center of the bundle for different values of G_m. In all cases the time constant τ_1 which governs the final part of the voltage response is distinctly shorter than the respective membrane time constant; however, the variation of τ_1 with varying values of G_m is relatively small. Half-time of potential change increases with decreasing membrane conductance and is between 0.1 and 0.2 ms.

Active Membrane; Response to Voltage Step

To study the behavior of a nonlinear membrane under double sucrose gap conditions, numerical computations were made on the model of a fiber bundle endowed with standard kinetics for fast Na conductance change. For simplicity, the K conductance was taken to be

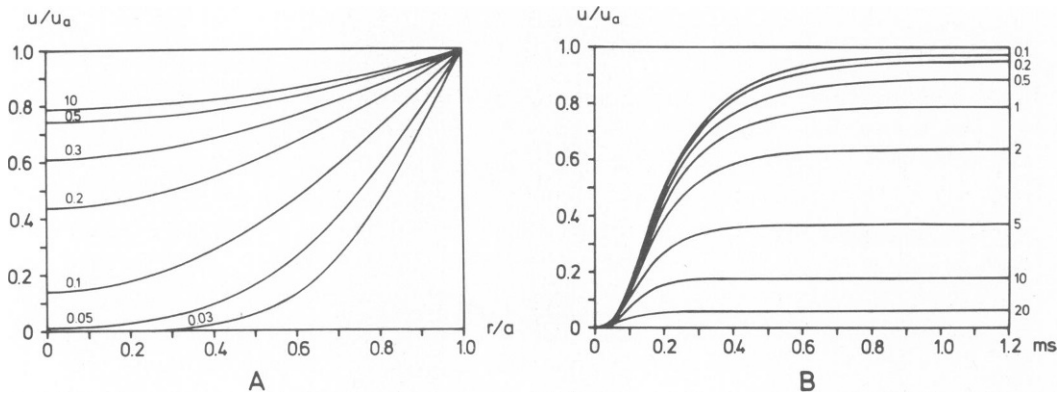

FIGURE 4 (A) Potential distribution in a frog atrial muscle strip at different times after sudden displacement of potential at bundle surface, starting from zero conditions. Abscissa: radial distance plotted as fraction of bundle radius; ordinate: potential as fraction of surface potential step. Membrane conductance and capacitance were taken to be 1 mmho/cm^2 and 1 μF/cm^2, respectively. The numbers on each curve are time in millseconds after onset of voltage clamp. (B) Influence of membrane conductance (G_m) on voltage response in the central fibers of a frog atrial bundle to a step change in potential at bundle surface. Abscissa: time after onset of voltage clamp; ordinate: potential as fraction of surface potential step. Curves are computed from Eq. 17 for $r = 0$ and values of G_m between 0.1 and 20 mmho/cm^2 as indicated at the right end of each curve. $C_m = 1$ μF/cm^2.

constant and ionic components of membrane current other than Na or K were neglected. With these assumptions Eq. 4 becomes

$$\frac{\partial^2 V}{\partial r^2} + \frac{1}{r}\frac{\partial V}{\partial r} = \frac{4}{d\sigma_e}[g_{Na}(V - V_{Na}) + g_K(V - V_K) + C_m \partial V/\partial t] \qquad (4a)$$

where the absolute membrane potential E has been substituted by V, the displacement of membrane potential from its resting value. The Hodgkin-Huxley (1952*b*) formulation was used to describe the Na conductance as a function of voltage and time. (Note that the terminology employed in this section is identical to the original Hodgkin-Huxley notation: inward current is taken positive and a negative value of V means a depolarization from the resting level.) The following values were adopted for the basic constants: a, bundle radius, 3×10^{-3} cm; d, cleft width, 3×10^{-6} cm; σ_e, conductivity of external medium, 11.5 mmho/cm; C_m, membrane specific capacitance, 2 μF/cm^2; V_{Na}, sodium equilibrium potential, -115 mV; V_K, potassium equilibrium potential, $+2.5$ mV; $\bar{g}_{Na}$, maximum sodium conductance, 120, 10, and 1 mmho/cm^2; g_K, potassium conductance, 0.5 mmho/cm^2. The potassium conductance was chosen to give a resting membrane resistance close to 2,000 Ωcm^2 and a net membrane current ($I_{Na} + I_K$) equaling zero at the resting level with $\bar{g}_{Na} = 120$ mmho/cm^2. All voltage clamp calculations were referred to initial resting conditions ($V = 0$; $m_\infty(0) = 0.053$; $h_\infty(0) = 0.6$).

The parabolic partial differential Eq. 4*a* was converted to discrete form by approximating the space derivatives on the left-hand side by the centered second and first difference at time t, respectively, and the time derivative on the right-hand side by the forward difference at distance r. The resulting forward difference equation was solved by a simple explicit method (Smith, 1969). Stability conditions were met by using integration time steps much shorter than the time constants of Na conductance change and by setting a suitable ratio of the increments in time and radial distance (cf. Ames, 1977). The radial increment was taken as $a/32$ and the time increment was in the order of 0.5 μs. The calculations were done on an IBM/370-168 computer.

The results obtained with $\bar{g}_{Na} = 120$ mmho/cm^2 will be considered first. Fig. 5 A illustrates the time-courses of membrane potential at different radial distances after application of a 50-mV step depolarization to the bundle. During the first few tenths of a millisecond after onset of the clamp, depolarization spreads from the surface to the center of the bundle as is expected from passive, resting membrane properties. If membrane conductance were to remain near g_K, the membrane potential of the central fibers would tend to a steady level of about -44 mV (cf. Eq. 6 and Fig 2 A), that is, a moderate hyperpolarization relative to the command voltage. After about half a millisecond, however, Na conductance steeply increases and the membrane potential of the inner fibers far overshoots the clamp potential. In fibers with a radial distance shorter than $a/2$, peak voltage, V_p, comes close to the Na equilibrium potential. Those fibers are actually out of control. The overshoot is still as large as 10 mV at $r/a = 0.96$. A sufficient voltage control is restricted to the outermost fibers of the bundle. Because of the nonuniformity of membrane potential, peak Na conductance, g_p, is not constant throughout the preparation; the respective values are 21 and 36.5 mmho/cm^2 at the surface and at the center of the bundle. Time to peak Na conductance is ~0.8 ms for the superficial fibers and 1 ms in the bundle axis. The falling phase of overshoot leads to a level

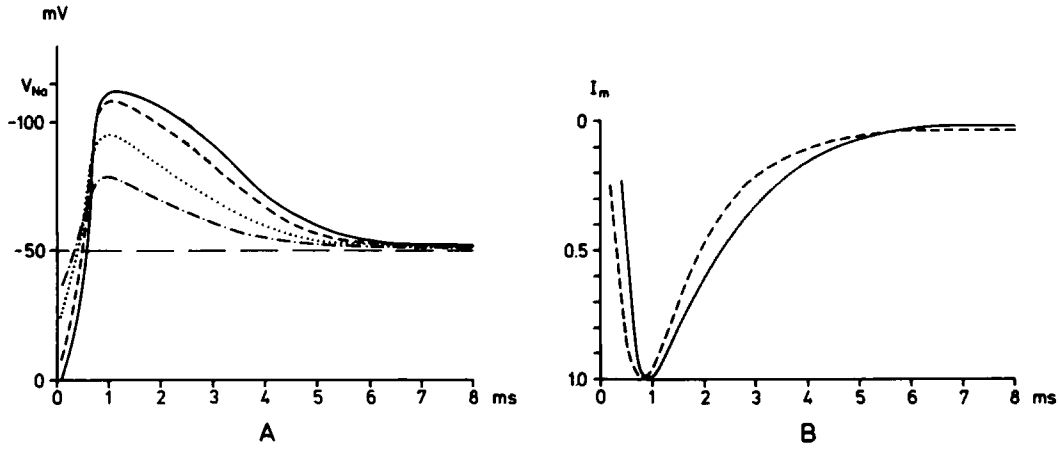

FIGURE 5 (A) Transmembrane voltage changes inside an active fiber bundle after application of a 50-mV step depolarization to the bundle surface. Abscissa: time after onset of clamp; ordinate: potential displacement from resting level at various radial distances, r/a = 0 (solid curve); 0.5 (dashed curve); 0.75 (dotted curve); 0.875 (dot-dashed curve); 1 (interrupted horizontal line). $\bar{g}_{Na}$ = 120 mmho/cm^2. (B) Early clamp currents of an active fiber bundle (full line) and of a free patch of membrane (dashed line) associated with a 50-mV step depolarization. Curves are normalized with respect to peak current value. The clamp current of the bundle was calculated according to Eq. 1*a*.

slightly above the command potential. (When the terms "above" and "below" are used to describe the relative position of two membrane potentials, it is meant that the upper level is depolarized relative to (in our terminology more negative than) the lower one.) This is the result of a small amount of Na conductance increase (~0.6 mmho/cm^2) persisting after inactivation (cf. Noble, 1966). In spite of the inadequacies of voltage control, the kinetics of the inward current wave are not grossly distorted. Fig. 5 B shows the total clamp current (in relative units) and the corresponding membrane current of a single space-clamped patch of membrane endowed with the same Na and K conductances but without any external series resistance. There is only a slight difference in the time to peak inward current and the apparent time constant of Na inactivation is ~1.4 ms for the bundle compared to 1.15 ms in the control.

Computations similar to those illustrated in Fig. 5 A were done for depolarizing voltage steps of varying amplitude. With strong depolarizations, peak Na conductance was almost constant across the bundle, regardless of the voltage deviations, and the radial profile of peak voltage was closely fitted by the steady-state voltage distribution calculated from Eq. 6 by setting $G_m = g_p$, $u = (V - V_{Na})$ and $u_a = (V_{clamp} - V_{NA})$. An example is shown in Fig 6.

Clamp current density at the bundle surface is given by

$$j_{clamp} = \frac{d\sigma_e}{b\sqrt{3}}\left(\frac{\partial V}{\partial r}\right)_a. \tag{1a}$$

Because 1 cm^2 of bundle surface is equivalent to $2a/(b\sqrt{3})$ cm^2 of actual membrane area, the mean value of membrane current density is

$$I_m = \frac{d\sigma_e}{2a}\left(\frac{\partial V}{\partial r}\right)_a. \tag{19}$$

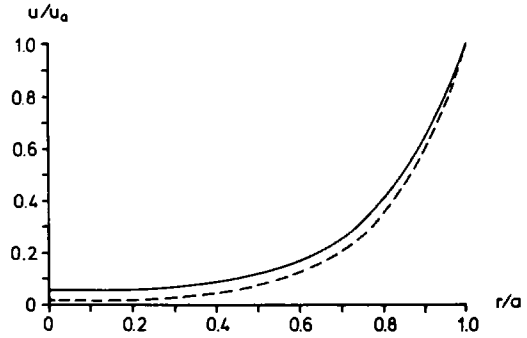

FIGURE 6 Solid line: Peak voltage profile across an active fiber bundle computed for an 80-mV step depolarization of the bundle surface. Abscissa: radial distance in relative units; ordinate: peak voltage at r expressed as the difference $u = (V_p - V_{Na})$ divided by the reference value of bundle surface, $u_a = (V_{clamp} - V_{Na})$. Peak Na conductance is between 35 (at the bundle surface) and 37 mmho/cm^2 (at the center). Interrupted line: Steady voltage profile in a passive fiber bundle calculated from Eq. 6 with $G_m = 36$ mmho/cm^2 (corresponding to $ak = 6.13$).

In our analysis the factor $d\sigma_e/(2a)$ was 5.75×10^{-3} mmho/cm and the derivative $(\partial V/\partial r)$ was approximated by the difference $V(a) - V(31/32\ a)$ divided by $a/32$.

Fig. 7 A shows a family of membrane currents, $I_m(t)$, computed for a series of step depolarizations ranging from 10- to 120-mV amplitude. At first glance the membrane current pattern resembles what one would expect from a proper clamp. A detailed inspection, however, reveals typical aberrations from ideal space clamping. In Fig. 7 B the peak early currents, I_p, taken from Fig. 7 A are plotted vs. the membrane potential during clamp, together with the ideal current-voltage relation for a membrane patch. Both curves intercept the voltage axis very close to the Na equilibrium potential. The most obvious alterations seen for the I-V relation of the bundle are (a) an exaggerated steepness of the negative slope region, combined with a shift of maximum I_p to the left of the voltage axis, (b) a depression of the maximum value of I_p and (c) a decreased slope of the positive region of the current-voltage curve. Because of the shift of the curve, there is a range of potential at which peak current density of the bundle is larger than the control and another at which it is smaller than the control.

A maximum Na conductance, $\bar{g}_{Na}$, of 120 mmho/cm^2 as derived from squid axon data might be an overestimation for structures of working myocardium. According to Beeler and Reuter (1977) the fully activated Na conductance of mammalian ventricular fibers, assessed from the action potential spike, is not more than ~4 mmho/cm^2 (see also the values reported by McAllister et al. [1975] and Schoenberg and Fozzard [1979] for Purkinje fibers). For the frog heart a similar estimation seems valid. Maximum rising velocity of the ventricular action potential was found to be as low as 20–50 V/s (Antoni and Delius, 1965; Niedergerke and Orkand, 1966); similar, or even lower, values apply to frog atrial muscle (Kern et al., 1971; de Hemptinne, 1976). Assuming that the membrane current during the rising phase is mainly carried by Na ions and membrane capacitance is 1–2 μF/cm^2, maximum Na current during the upstroke amounts to 100 μA/cm^2 or less, corresponding to a peak Na conductance of 1–2 mmho/cm^2. Thus it seems reasonable to set $\bar{g}_{Na}$ to a relatively small value of 10 mmho/cm^2 for the case of frog atrial muscle.

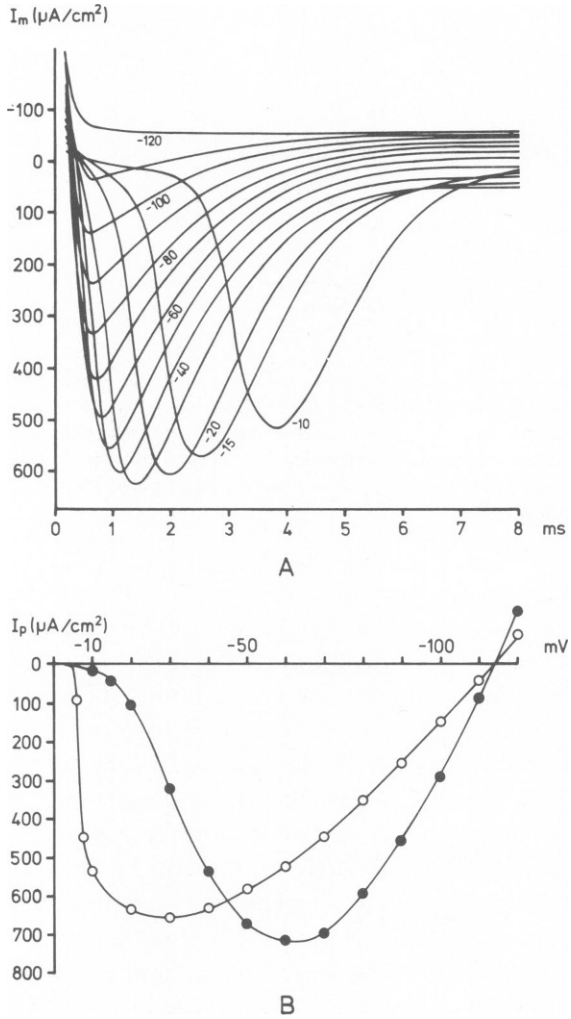

FIGURE 7 (A) Membrane currents of an active fiber bundle at various step depolarizations. Abscissa: time after onset of clamp; ordinate: mean membrane current density referred to actual membrane area. Numbers on the curves are depolarizations from resting level (in millivolts). $\bar{g}_{Na}$ = 120 mmho/cm². (B) Comparison between the peak inward current-voltage relations for a fiber bundle (open symbols) and for an active patch of membrane with no series resistance (filled symbols). Data are referred to zero current. Patch current is shown in half its actual value.

Fig. 8 A shows the computed voltage distribution in a frog atrial preparation after a 50-mV step depolarization. Regenerative Na activity is still present but strongly reduced compared with the case treated above (Fig. 5 A). The overshoot reaches 14 mV at the bundle axis. The steady potential attained at the end of the clamp is a small hyperpolarization with respect to the command voltage, indicating a predominance of g_K over the residual g_{Na}. Peak Na conductance, g_p, is almost constant throughout the bundle (1.75 and 1.85 mmho/cm² at the surface and at the center, respectively). Fig. 8 B presents the mean membrane current of the bundle and the control current of a single patch of membrane under ideal clamp conditions

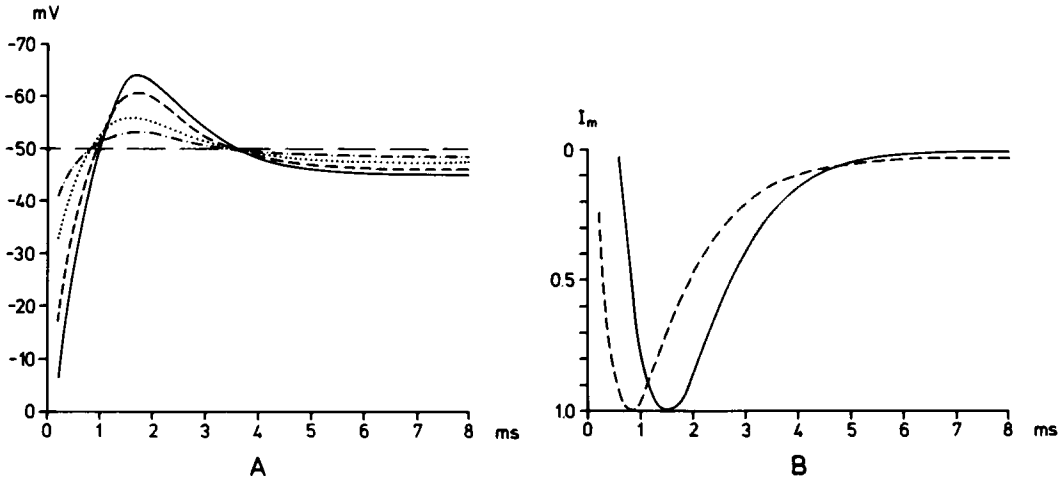

FIGURE 8 (A) Transmembrane voltage changes in a frog atrial fiber bundle in response to a 50-mV step clamp. Curves are labeled as in Fig. 5 A. $\bar{g}_{Na}$ = 10 mmho/cm^2. (B) Full line: early clamp current of a frog atrial bundle (referred to the level of steady outward current); dashed line: fast Na inward current of a free membrane patch during a 50-mV step depolarization.

(normalized configuration). The time-course of Na inactivation, assessed from the decay of inward current, is almost the same in the two tracings. Time to peak inward current is ~1.5 ms for the bundle and 0.8 ms in the control. When comparing Figs. 5 B and 8 B, we see that for a smaller value of $\bar{g}_{Na}$ the apparent time-course of Na activation is more delayed relative to the true H-H kinetics than for a high value of $\bar{g}_{Na}$ (cf. Fig. 3 *b* in Jakobsson et al., 1975). This appears to be because the turn on of Na current which helps to depolarize the deeper-lying membranes is less effective in case of a lower Na conductance. Different rates of depolarization of the inner fibers at different values of $\bar{g}_{Na}$ are clearly seen in Figs. 5 A and 8 A.

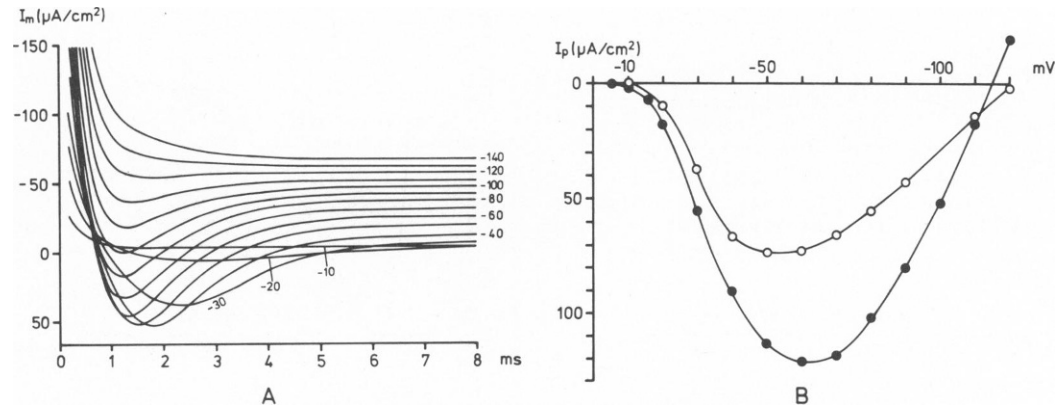

FIGURE 9 (A) Membrane current simulations for a frog atrial fiber bundle; $\bar{g}_{Na}$ = 10 mmho/cm^2. The clamp potential was varied in 10-mV steps. Numbers against the curves are depolarizations from resting level. (B) Current-voltage diagrams for peak early inward current of a frog atrial bundle (○) and for peak I_{Na} of a free membrane patch (●). The current data of the bundle are referred to the respective steady outward currents.

Fig. 9 A shows a family of membrane currents computed for step depolarizations of 10–140 mV amplitude. The 10-mV step is a "subthreshold" depolarization and the current tracing is very similar to the response predicted by Eq. 18 for G_m = 0.5 mmho/cm^2. With higher depolarizations, downward deflections occur resembling Na inward current waves. An unexpected finding is that the 120-mV clamp which is nominally above the Na equilibrium potential produces a transient *inward* current (relative to steady current) rather than the presumed transient outward current. This phenomenon is understood by the following consideration. The intrinsic electromotive force resulting from constant g_K (= 0.5 mmho/cm^2) and activated g_{Na} in the order of 4 mmho/cm^2 is about −102 mV. The membrane potential of interior fibers which are not adequately controlled therefore tends to values below −115 mV. Actually, the membrane potential does not exceed −107 mV in the axis of the bundle. Thus the central fibers will produce a Na inward current. There is only a thin layer of cells that are at membrane potentials above −115 mV, thereby generating an outward Na flow. Fig. 9 B shows the peak inward current-voltage relation for the bundle and the corresponding plot for a membrane patch under ideal conditions. Again the current-voltage curve of the bundle exhibits a shift of maximum I_p in the hyperpolarizing direction and a decreased size and slope over the positive region. However, the deviations from ideal configuration are less pronounced than those seen in Fig. 7 B. The positive limb of the *I-V* curve projects a reversal potential which is clearly beyond the Na equilibrium potential. (A similar phenomenon was described by Jakobsson et al., 1975).

Finally, the case of a very low conductance, $\bar{g}_{Na}$ = 1 mmho/cm^2 will be considered. This case might be of interest for experimental conditions in which most of the Na channels are blocked by tetrodotoxin. Furthermore, a conductance of 0.25 mmho/cm^2 has been assumed for the secondary, slow inward current in myocardial tissue (Bassingthwaighte and Reuter, 1972). Fig. 10 A illustrates the computed voltage pattern in a frog atrial bundle during a 50-mV step depolarization. At all times the inner fibers are hyperpolarized with respect to the command voltage; activation of the Na system is manifested by a small (<3 mV) overshoot relative to the steady-state potential. Peak inward current conductance, g_p, is 0.175 and 0.134

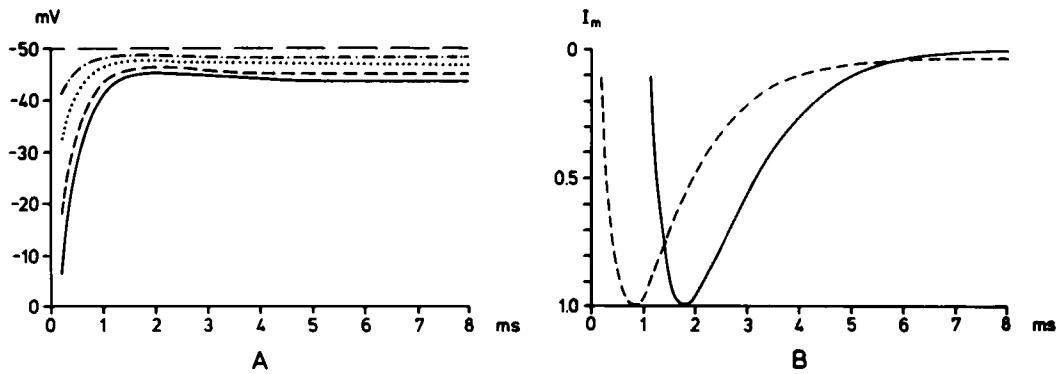

FIGURE 10 (A) Transmembrane voltage changes across a frog atrial fiber bundle with a very low Na conductance ($\bar{g}_{Na}$ = 1 mmho/cm^2) during a 50-mV step clamp. Curves are labeled as in Fig. 5 A. (B) Full line: early inward current of the bundle (referred to the level of steady outward current); dashed line: control current of a free membrane patch during a 50-mV depolarization. Both curves are normalized with respect to their peak values.

at the surface and the center of the bundle, respectively. The observation that g_p is smaller in central fibers than in peripheral fibers at $\bar{g}_{Na} = 1$ mmho/cm^2 contrasts to what has been found with $\bar{g}_{Na} = 10$ or 120 mmho/cm^2. The difference is explained by the fact that the peak potential of the inner fibers is below the command level with $\bar{g}_{Na} = 1$ mmho/cm^2 whereas it is above this level with the higher conductances (Fibs. 5 A and 8 A). In Fig. 10 B the mean membrane current of the bundle and the control current of a single patch of membrane are shown. Again the time-course of decay of inward current is almost the same in the two tracings, with a delay of ~1 ms for the bundle current. Fig. 11 A presents the membrane currents of the bundle associated with clamps of 10–130 mV amplitude. At any level of depolarization net current is directed outward throughout the clamp. Between 20 and 110 mV small downward deflections, representing transient inward current, are superimposed on the current pattern resulting from capacitive and steady K current. Time to peak inward current is in the order of 2 ms, that is, development of inward current is slowed by a factor of 2–5 compared to the true H-H kinetics. This error is similar to, but more pronounced than, the apparent delay of Na activation observed with the higher conductances. Fig. 11 B depicts the peak inward current-voltage relation of the bundle and the control curve of a membrane patch at $\bar{g}_{Na} = 1$ mmho/cm^2. The error in size of inward current is of the same order as was found with $\bar{g}_{Na} = 10$ mmho/cm^2.

DISCUSSION

The above simulations clearly demonstrate the inadequacies inherent in voltage or current clamp experiments on multicellular, bundle-like structures in a double sucrose gap. The presence of a marked resistance in the intercellular clefts prevents a strict uniformity of membrane current and potential across the bundle, thereby introducing systematical deviations from ideal space clamping. The question then is whether the irreducible errors in voltage or current control may be accounted for and conclusions can be drawn regarding actual membrane properties.

Resting membrane parameters are investigated by application of small voltage or current steps which do not significantly alter the state of the membrane. The current and voltage

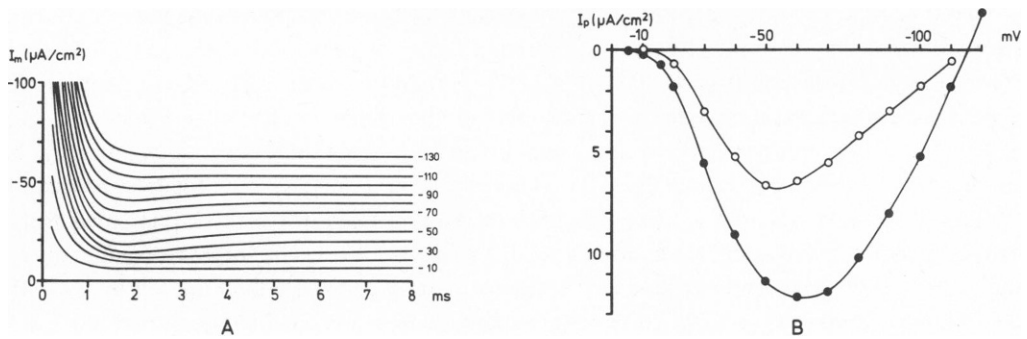

FIGURE 11 (A) Clamp currents of a fiber bundle with $\bar{g}_{Na} = 1$ mmho/cm^2 during step depolarizations of varying amplitude. Depolarization from resting level (in millivolts) is given at the end of each current tracing. (B) Comparison of the peak inward current-voltage relations for the fiber bundle (o) and for a free patch of membrane (•). Current data of the bundle are referred to the respective steady outward currents.

responses may be evaluated by the analytical approach described in Results provided that the geometry of the preparation (bundle radius a, fiber radius b, cleft width d, node length l) and the conductivity of the extracellular fluid (σ_e) are known. The measured total clamp current of a cylindrical bundle is related to the mean membrane current density by the factor $4\pi a^2 l/(b\sqrt{3})$. The time-independent values of membrane current density (I_m) and membrane potential at the bundle surface (u_a) yield the apparent membrane conductance ($\bar{G} = I_m/u_a$). The relation between $\bar{G}$ and the true membrane conductance (G_m) is determined by Eq. 8*b*. With given values of a, d, and σ_e, the right-hand side of this equation is a (monotonical) function of G_m (because $k = 2\sqrt{G_m/d\sigma_e}$). Unfortunately, Eq. 8*b* cannot be solved explicitly for G_m. It is therefore necessary to determine G_m from a $\bar{G}$ vs. G_m plot as is shown in Fig. 2 B for a frog atrial preparation. From a semilog plot of the transients related to the onset of a current step, the membrane time constant ($\tau = C_m/G_m$) and consequently the membrane capacitance (C_m) can be obtained (cf. Fig. 3 B). The transients related to a voltage step may also be used to estimate τ or C_m (cf. Eq. 18).

It should be emphasized that, for practical purposes, the above correction procedure for determination of steady membrane conductance is not more than a rough approximation. The correction factor derived in the present study depends on several parameters which may not be uniform throughout a real preparation (e.g. cleft size and external conductivity) and implies a number of assumptions (e.g. isopotentiality of the fiber interior) which are not strictly realized under sucrose gap conditions. Thus the "corrected" data will still be erroneous to some extent.

The parameters of an active, nonlinear membrane are more difficult to elaborate. From the computations presented above it is obvious that, in general, voltage clamp experiments on a fiber bundle do not allow a complete, quantitative analysis of early excitatory inward current. However, a rough estimation of some parameters of the Na system might be achieved. A parameter of particular interest is the limiting Na conductance, g'_{Na}, i.e., the maximum value of Na conductance that can be attained by strong depolarizations from the resting level. Under ideal clamp conditions, g'_{Na} is essentially equivalent to the slope conductance of the positive region of the peak inward current-voltage relationship. In a multifiber preparation with a high Na conductance (e.g. $\bar{g}_{Na}$ = 120 mmho/cm^2) all fibers will undergo a rapid potential change and any individual fiber may reach a peak Na conductance near g'_{Na} during strong depolarizing clamps. However, the driving force for peak Na current, $(V_p - V_{Na})$, is much smaller for the poorly controlled interior fibers than for the properly clamped superficial ones. This is a direct consequence of the distinct voltage overshoot of the inner fibers (cf. Fig. 5 A). Thus the apparent positive slope conductance, $\bar{G}_{sl}$, obtained from a bundle will be smaller than the true g'_{Na} value (Fig. 7 B). This error could be accounted for by a procedure analogous to the correction on resting membrane data outlined in the preceding paragraphs. Provided that the activated Na conductance far exceeds all other membrane conductances, the peak voltage profile related to a strong depolarization may be approximated by a steady potential distribution as would result with a constant membrane conductance equal to g'_{Na} (cf. Fig. 6). With this assumption, g'_{Na} can be read off from an appropriate $\bar{G} - G_m$ curve. As an example, we consider the *I-V* relations shown in Fig. 7 B. In this case the positive slope conductance of the bundle is ~11.5 mmho/cm^2 whereas the slope conductance of the control amounts to ~43 mmho/cm^2. On the other hand, a membrane conductance of 40 mmho/cm^2 is

obtained from the $\overline{G}$ vs. G_m plot in Fig. 2 B at an apparent membrane conductance of 11.5 mmho/cm^2. (The approximative nature of the correction procedure should be stressed again.) In a preparation with a low Na conductance, the situation is more complex. With $\bar{g}_{Na}$ = 1 mmho/cm^2, the driving force for peak Na current during depolarizing clamps is larger in the inner fibers than in the periphery of the bundle but depolarization of the inner fibers is so much delayed that appreciable part of the Na conductance is inactivated before the peak is reached (Figs. 10 A, B). Because of this inactivation, the mean membrane current over the positive limb of the peak current-voltage relation is again smaller than the control current (Fig. 11 B).

The difference between the reciprocal values, $1/\overline{G}_{sl}$ and $1/g'_{Na}$, may be interpreted as the effective extracellular resistance of a bundle to radial current flow. With the values cited for $\bar{g}_{Na}$ = 120 mmho/cm^2, the effective series resistance comes to about (1/11.5) − (1/43) = 0.064 kΩcm^2 = 64 Ωcm^2. This value is smaller by one order of magnitude than the lumped series resistance proposed by Kootsey and Johnson (1972) in their single fiber model of ventricular muscle (500 Ωcm^2). In that model (which is also based on a maximum Na conductance, $\bar{g}_{Na}$, of 120 mmho/cm^2) the positive slope conductance of the peak inward current-voltage relation is not more than 1.7 mmho/cm^2 which is nearly identical to the 2 mmho/cm^2 expected from the series resistance alone (cf. Fig. 4 A of their paper). This led the authors to the statement "that the shape of the peak current-voltage plot tells us almost nothing about the membrane properties." The results presented here suggest that the significance of Na current measurements on bundle-like structures may not be as poor as inferred by Kootsey and Johnson. In our model the discrepancy between the apparent Na conductance ($\overline{G}_{sl}$) and the actual value (g'_{Na}) is about fourfold rather than in the order of 25-fold as is predicted by the Kootsey-Johnson model. For the frog atrial preparation with a lower Na conductance ($\bar{g}_{Na}$ = 10 mmho/cm^2) the discrepancy is reduced to about twofold (cf. Fig. 9 B).

Furthermore, there are some properties of the Na system which are usually determined from Na current spike ratios rather than absolute Na currents. For a fiber bundle those measurements would seem to be meaningful provided that the relative error (the percent deviation of the measured peak I_{Na} from the ideal value expected in the absence of external series resistance) is almost constant in the Na spikes to be compared. Under these conditions, a correction of the individual Na currents would be dispensible. For example, the time-course of Na reactivation at the resting level (= recovery from inactivation after cessation of a depolarizing clamp) could be pursued by the conventional pulse arrangement consisting of two identical depolarizing clamps applied at various intervals (Hodgkin and Huxley, 1952*a*). Assuming that (*a*) depolarization is strong enough to produce full activation of the Na system in any fiber of the bundle, (*b*) the time required for full repolarization of any fiber after the break of the conditioning pulse is short relative to the duration of the interval and (*c*) the factor relating peak I_{Na} and g_p is essentially the same for the conditioning pulse and the test pulse, the spike ratio would give a reasonable approximation of the g_p ratio and the degree of recovery attained at the beginning of the test pulse could be determined as a function of the time interval between the two pulses. The first and the second condition may be met by a proper choice of the pulse arrangement. The third condition cannot be strictly fulfilled because the relation between peak I_{Na} and g_p is expected to vary with the absolute amount of

Na conductance. However, this error can be minimized by considering only those test spikes which are not too small relative to the reference spike. For a test spike which is two-thirds of the reference value, the actual g_p ratio would be between one-half and two-thirds. This estimation is based on the assumption that the relation between peak I_{Na} and g_p is similar to the $\overline{G} - G_m$ curve shown in Fig. 2 B. For smaller test spikes, a theoretical correction of both reference and test spike would be necessary. A similar problem is the determination of the steady-state Na inactivation (h_∞) curve from normalized Na current spikes related to various prepotentials.

Another parameter which could be estimated from voltage clamp experiments on a fiber bundle is the maximum rate of the Na inactivation process. In the simulations presented above, the time-courses of inward current decay during a depolarization of 50 mV or more were quite similar on the fiber bundle and in the controls (cf. Figs. 5 B and 8 B). This is mainly a result of the fact that the time constant of Na inactivation (τ_h), as a function of membrane potential, approaches a constant minimum (~1 ms in the H-H formulation) with increasing depolarization. (The respective values for $V = -50$ and -60 mV are 1.15 and 1.05 ms.) Thus a voltage overshoot of the inner fibers in response to a step depolarization of the bundle surface is not expected to cause a serious distortion of the Na inactivation kinetics and an analysis of the falling phase of inward current is likely to give an approximate value of minimal τ_h.

We would like to thank Dr. C. Achenbach for his careful reading of this paper and his helpful comments. We also appreciate the collaboration of Mr. H. Förster from the Department for Applied Mathematics of the University of Bonn in the explicit integrations for active membrane responses.

Received for publication 26 November 1979.

REFERENCES

ADRIAN, R. H., W. K. CHANDLER, and A. L. HODGKIN. 1969. The kinetics of mechanical activation in frog muscle. *J. Physiol. (Lond.).* **204**:207–230.

AMES, W. F. 1977. Numerical Methods for Partial Differential Equations. Academic Press, Inc., New York.

ANTONI, H., and W. DELIUS. 1965. Nachweis von zwei Komponenten in der Anstiegsphase des Aktionsptentials von Froschmyokardfasern. *Pfluegers Archiv. Gesamte Physiol. Menschen Tiere.* **283**:187–202.

ATTWELL, D., and I. COHEN. 1977. The voltage clamp of multicellular preparations. *Prog. Biophys. Mol. Biol.* **31**:201–245.

BALDWIN, K. M. 1970. The fine structure and electrophysiology of heart muscle cell injury. *J. Cell Biol.* **46**:455–476.

BARR, L., M. M. DEWEY, and W. BERGER. 1965. Propagation of action potentials and the structure of the nexus in cardiac muscle. *J. Gen. Physiol.* **48**:797–823.

BASSINGTHWAIGHTE, J. B., and H. REUTER. 1972. Calcium movements and excitation-contraction coupling in cardiac cells. *In* Electrical Phenomena in the Heart. W. C. De Mello, editor. Academic Press, Inc., New York. 353–395.

BEELER, G. W., and H. REUTER. 1977. Reconstruction of the action potential of ventricular myocardial fibres. *J. Physiol. (Lond.).* **268**:177–210.

CONNOR, J., L. BARR, and E. JAKOBSSON. 1975. Electrical characteristics of frog atrial trabeculae in the double surcose gap. *Biophys. J.* **15**:1047–1067.

DE HEMPTINNE, A. 1976. Voltage clamp analysis in isolated cardiac fibres as performed with two different perfusion chambres for double sucrose gap. *Pfluegers Archiv. Gesamte Physiol. Menschen Tiere.* **363**:87–95.

DOETSCH, G. 1967. Anleitung zum praktischen Gebrauch der Laplace-Transformation und der Z-Transformation. Oldenbourg Verlag, Munich and Vienna.

EISENBERG, R. S., V. BARCILON, and R. T. MATHIAS. 1979. Electrical properties of spherical syncytia. *Biophys. J.* **25**:151–180.

FITZHUGH, R. 1960. Thresholds and plateaus in the Hodgkin-Huxley nerve equations. *J. Gen Physiol.* **43**:867–896.

HODGKIN, A. L., and A. F. HUXLEY. 1952*a*. The dual effect of membrane potential on sodium conductance in the giant axon of Loligo. *J. Physiol. (Lond.).* **116**:497–506.

HODGKIN, A. L., and A. F. HUXLEY. 1952*b*. A quantitative description of membrane current and its application to conduction and excitation in nerve. *J. Physiol. (Lond.).* **117**:500–544.

JAKOBSSON, E., L. BARR, and J. A. CONNOR. 1975. An equivalent circuit for small atrial trabeculae of frog. *Biophys. J.* **15**:1069-1085.

JOHNSON, E. A., and M. LIEBERMAN. 1971. Heart: excitation and contraction. *Annu. Rev. Physiol.* **33**:479–532.

JULIAN, F. J., J. W. MOORE, and D. E. GOLDMAN. 1962*a*. Membrane potentials of the lobster giant axon obtained by use of the sucrose-gap technique. *J. Gen. Physiol.* **45**:1195–1216.

JULIAN, F. J., J. W. MOORE, and D. E. GOLDMAN. 1962*b*. Current-voltage relations in the lobster giant axon membrane under voltage clamp conditions. *J. Gen. Physiol.* **45**:1217–1238.

KERN, R., H. M. EINWÄCHTER, H. G. HAAS, and E. G. LACK. 1971. Cardiac membrane currents as affected by a neuroleptic agent: droperidol. *Pfluegers Archiv. Gesamte Physiol. Menschen Tiere.* **325**:262–278.

KOOTSEY, J. M., and E. A. JOHNSON. 1972. Voltage clamp of cardiac muscle. A theoretical analysis of early currents in the single sucrose gap. *Biophys. J.* **12**:1496–1508.

MCALLISTER, R. E., D. NOBLE, and R. W. TSIEN. 1975. Reconstruction of the electrical activity of cardiac Purkinje fibres. *J. Physiol. (Lond.).* **251**:1–59.

MCGUIGAN, J. A. S. 1974. Some limitations of the double sucrose gap, and its use in a study of the slow outward current in mammalian ventricular muscle. *J. Physiol. (Lond.).* **240**:775–806.

NIEDERGERKE, R., and R. K. ORKAND. 1966. The dual effect of calcium on the action potential of the frog's heart. *J. Physiol. (Lond.).* **184**:291–311.

NOBLE, D. 1966. Applications of Hodgkin-Huxley equations to excitable tissues. *Physiol. Rev.* **46**:1–50.

PAGE, S. G., and R. NIEDERGERKE. 1972. Structures of physiological interest in the frog heart ventricle. *J. Cell Sci.* **11**:179–203.

PESKOFF, A. 1979*a*. Electric potential in three-dimensional electrically syncytial tissues. *Bull. Math. Biol.* **41**:163–181.

PESKOFF, A. 1979*b*. Electric potential in cylindrical syncytia and muscle fibers. *Bull. Math. Biol.* **41**:183–192.

RAMÓN, F., N. ANDERSON, R. W. JOYNER, and J. W. MOORE. 1975. Axon voltage clamp simulations. IV. A multicellular preparation. *Biophys. J.* **15**:55–69.

SCHOENBERG, M., and H. A. FOZZARD. 1979. The influence of intercellular clefts on the electrical properties of sheep cardiac Purkinje fibers. *Biophys. J.* **25**:217–234.

SHANES, A. M. 1958. Electronchemical aspects of physiological and pharmacological action in excitable cells. II. The action potential and excitation. *Pharmacol. Rev.* **10**:165–273.

SMITH, G. D. 1969. Numerical Solution of Partial Differential Equations. The Oxford University Press, London.

SOMMER, J. R., and E. A. JOHNSON. 1968. Cardiac muscle: a comparative study of Purkinje fibers and ventricular fibers. *J. Cell Biol.* **36**:497–526.

TARR, M., and J. W. TRANK. 1974. An assessment of the double sucrose-gap voltage clamp technique as applied to frog atrial muscle. *Biophys. J.* **14**:627–643.

TARR, M., and J. W. TRANK. 1976. Limitations of the double sucrose gap voltage clamp technique in tension-voltage determinations on frog atrial muscle. *Circ. Res.* **39**:106–112.